Journal of The Electrochemical Society, **155** (5) B483-B487 (2008)
0013-4651/2008/155(5)/B483/5/$23.00 © The Electrochemical Society

Synthesis and Electrical Characterization of the Ceramic Anode $La_{1-x}Sr_xMn_{0.5}Cr_{0.5}O_3$

F. C. Fonseca,[a,z] E. N. S. Muccillo,[a,*] R. Muccillo,[a,*] and D. Z. de Florio[b]

[a]*Instituto de Pesquisas Energéticas e Nucleares, 05508-000 São Paulo, SP, Brazil*
[b]*Universidade Federal do ABC, 09210-170 Santo André, SP, Brazil*

The synthesis and electrical characterization of $La_{1-x}Sr_xMn_{0.5}Cr_{0.5}O_3$ compounds are reported. These compounds, with perovskite structure, have been pointed out as a promising alternative for the nickel-based cermet anode of solid oxide fuel cells. Polycrystalline samples, with $x = 0.3$, 0.4, and 0.5, were prepared by the citrate technique. The crystalline phase and the chemical compatibility with zirconia-based electrolytes were studied by X-ray diffraction analyses. The electrical properties were studied by four-probe dc electrical conductivity $\sigma(T)$ measurements during redox cycles under both oxidizing and reducing atmospheres. The main results show that the $\sigma(T)$ has a thermally activated behavior, and increasing Sr content increases $\sigma(T)$. Compounds with $x = 0.3$ exhibited no appreciable chemical reaction with the stabilized zirconia electrolyte after heat-treatment at high temperature. The $\sigma(T)$ measurements evidenced the redox stability of the ceramic anode. However, some degradation of the $\sigma(T)$ was observed on samples thermally treated at 1000°C under pure hydrogen.
 [DOI: 10.1149/1.2885099]

Manuscript submitted December 13, 2007; revised manuscript received January 29, 2008.
Available electronically March 18, 2008.

Solid oxide fuel cells (SOFCs) have attracted a great deal of attention due to the possibility of clean generation of electrical energy with high efficiency.[1] An important advantage of SOFCs consists in their ability to use several primary fuels, such as hydrogen, methane, methanol, and gasified coal.[1,2] In this direction, a great research effort has been devoted to the improvement of the anode material, which is the electrode where the fuel reaction takes place.[2] The nickel+yttria-stabilized zirconia cermet has been the dominant SOFC anode for the last four decades.[1,2] Despite the good performance of this anode, some limitations are observed, mostly when carbon-containing fuels are used.[2] In these cases, the formation of carbon deposits usually occurs over the surface of the metal particles, resulting in severe degradation of the anode. This process has been limited by the circulation of an excess of steam in the anode but decreases the efficiency of the device. Other relevant drawbacks of the cermet are related to the low redox stability, thermal aging due to sintering of metallic particles, and the relatively high thermal expansion coefficient compared with the zirconia-based electrolyte one.[2,3]

Some alternative materials have been proposed as possible substitutes for the nickel-based cermets aiming at better redox stability and the use of hydrocarbon fuels. Ceramic oxides are promising candidates for this application, because they generally exhibit low catalytic activity for carbon deposition and, at the same time, they can display appreciable catalytic activity for the oxidation of hydrocarbon fuels.[3] However, such oxides normally have lower electric conductivity than those of the cermet and, in fact, the ideal oxide anode to replace Ni cermets has not yet been reported.[3]

In this context, the $La_{1-x}Sr_xCr_{0.5}Mn_{0.5}O_3$ (LSCM-x%) compounds have been pointed out as a possible candidate material for SOFC anode.[4,5] The LSCM-25 with $x = 0.25$ compound has the perovskite structure, is stable in reducing atmosphere, and exhibits low polarization resistance.[4,5] In addition, the Sr-doped lanthanum chromite–manganite does not catalyze carbon deposition and allows for the reformation of methane without excess steam.[3] Studies concerning the performance of these materials in single SOFC and the influence of the relative composition of Cr and Mn have been reported.[5-7] Moreover, systematic studies concerning the influence of the Sr content,[8] thermal aging in fuel conditions, and microstructural optimization of the ceramic may further contribute to the application of this perovskite as SOFC anode.

In this manuscript, synthesis by the citrate technique and characterization of the $La_{1-x}Sr_xCr_{0.5}Mn_{0.5}O_3$ compounds, with Sr composition in the range $0.3 \leq x \leq 0.5$, are presented. The compatibility of the ceramic anode with zirconia-based electrolytes was studied, and the stability of the compound during redox cycles was investigated by means of electrical resistivity measurements in different atmospheres in both as-sintered and H_2 thermally aged samples. The main results show that the composition with $x = 0.5$ shows the highest value of the electrical conductivity, but its use as a anode is restricted due to the chemical reaction with yttria-stabilized zirconia (YSZ) at high temperatures. Compounds with $x = 0.3$ have achieved relatively high values of electric conductivity, and no appreciable reaction with YSZ has been detected. In addition, this composition exhibits stable behavior during cycles of oxidation and reduction between the ambient temperature and the operation temperature of the SOFC.

Experimental

Ceramic samples of the LSCM-x% compound, with $x = 0.3$, 0.4, and 0.5, were prepared by the citrate (polymeric precursor) technique.[9] Initially, solutions of the starting materials, $MnCl_2 \cdot 4H_2O$, $Cr(NO_3)_3 \cdot 9H_2O$, $Sr(NO)_3$, and $La(NO)_3 \cdot 6H_2O$ (Sigma-Aldrich, PA), were prepared with deionized water and calibrated by weighing the oxide content after calcination of aliquots at 900°C. The amount of citric acid (CA) and ethylene glycol (EG) was fixed in the proportion 60:40 wt % (CA:EG). The resins were prepared by combining stoichiometric amounts of the starting solutions in the following sequence: $MnCl_2 \cdot 4H_2O$, $Cr(NO_3)_3 \cdot 9H_2O$, $Sr(NO)_3$, and $La(NO)_3 \cdot 6H_2O$. The resulting solution was heated at 60°C under magnetic stirring. After ~5 min, the CA was added and the solution was kept under constant stirring at 60°C. After ~1 h, a homogeneous solution of EG and an excess of 50 mol % of CA, which was previously maintained at 60°C under agitation for ~20 min, were added to the solution. Then, the temperature of the system was increased to ~100°C under continuous stirring for ~40 min until a viscous resin was obtained. The thermal decomposition of the polymeric resin was studied by means of simultaneous thermogravimetric (TG) and differential thermal (DTA) analyses up to 1400°C with a heating rate of 10°C/min in air (5 mL/min) in Setaram Labsys TG/DTA equipment. The resulting resin was thermally treated at 300°C for 4 h and calcined at 1000°C for 12 h in air. Cylindrical samples (10 mm diameter and ~1 mm thickness) were uniaxially pressed (1 ton/cm^2) and sintered at 1400°C for 12 h in air.

The characterization of the phases was performed by X-ray diffraction (XRD) analyses of both calcined and sintered powders, in the 2θ° range of 20–80°, with step size 0.05 (2θ°) and counting time of 2 s, with Cu Kα radiation in a Bruker-AXS D8 Advance

* Electrochemical Society Active Member.
[z] E-mail: cfonseca@ipen.br

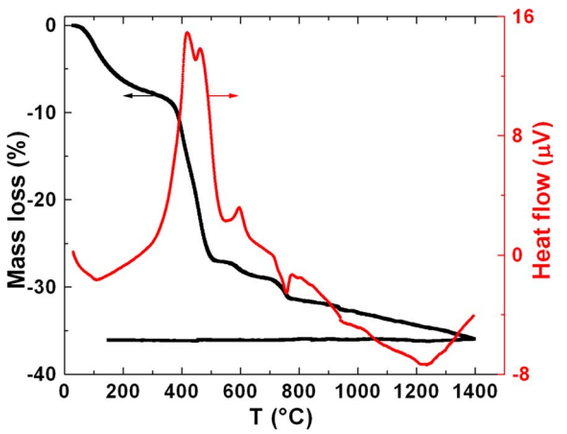

Figure 1. (Color online) TG (left axis) and DTA (right axis) of the precursor resin for the compound $La_{0.5}Sr_{0.5}Cr_{0.5}Mn_{0.5}O_3$.

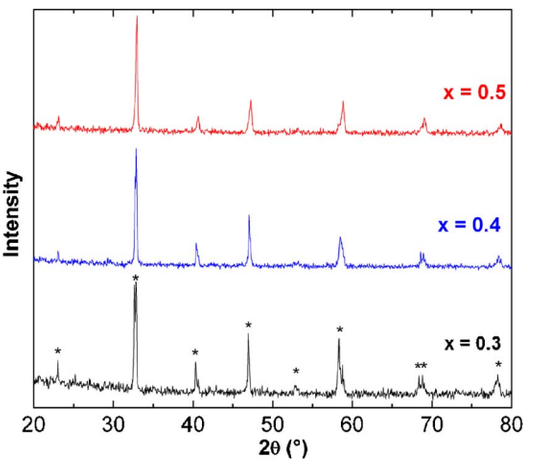

Figure 2. (Color online) Powder XRD patterns of sintered LSCM-*x*% compounds with $x = 0.3$, 0.4, and 0.5. The * symbol indicates the indexed peaks of the perovskite phase.

diffractometer. In addition, the reactivity of the perovskite with zirconia-based electrolytes was studied by mixing LSCM-*x*% and ZrO_2:8 mol % Y_2O_3 (Tosoh) powders in an agate mortar in the 1:1 weight proportion. The resulting mixture was treated at 1300°C for 5 h in air, and the reactivity of the materials was evaluated by means of XRD analyses.

The electric characterization was carried out in a system built for measuring the temperature dependence of the dc electrical resistivity [$\rho(T)$] by using the four-probe method. Such a system consists essentially of a vertical resistive furnace with controlled atmosphere and an Inconel 600 sample-holder equipped with a type-K thermocouple, alumina parts, and Pt wires. Measurements were performed with Keithley current source and digital multimeter, models 2400 and 2000, respectively. The experimental setup is controlled by a microcomputer through a general purpose bus interface. The sample preparation for $\rho(T)$ measurements involves cutting bar-shaped specimens (typically $8 \times 2 \times 1$ mm) in a diamond saw, depositing the contacts with Ag paste, and curing the contacts at 500°C/30 min. The $\rho(T)$ measurements were carried out in air and under a flowing gas mixture of 96% Ar/4% H_2 [$p(O_2) \approx 10^{-18}$ atm at 900°C] in the 100–800°C temperature range. The redox stability was further studied by $\rho(T)$ measurements of both samples sintered in air and samples thermally treated at 1000°C for 5 h under H_2 (~100 mL/min) in order to evaluate possible thermal aging effects in fuel conditions. TG analysis of powdered samples was carried out between room temperature and 800°C, at 10°C/min heating/cooling rates, under both air and 96% Ar/4% H_2 gas mixture to correlate the features of $\rho(T)$ data with mass variations.

Results and Discussion

Figure 1 shows the results of TG/DTA simultaneous analysis for the $x = 0.5$ (LSCM-50) precursor resin obtained by the citrate technique. Thermal decomposition occurs in four mains steps between room temperature and 800°C, i.e., at ~110, 440, 600, and 750°C, which are related to water, organic matter, and Cl^- ions release.[10] The total mass loss up to 800°C was ~31.5%, and further heating results in a rather slight mass loss of ~4% up to 1400°C. The DTA peaks are closely associated with mass-loss events, and samples with different Sr content show no significant differences regarding the TG/DTA results.

Figure 2 shows the results of the powder XRD analysis of the samples with $x = 0.3$, 0.4, and 0.5 after sintering at 1400°C. The observed XRD patterns displayed in Fig. 2 are similar to previously reported patterns for compounds $La_{1-x}Sr_xMnO_3$ (LSM) with equivalent Sr content.[5-7,11] It has been assumed that the LSCM-*x*% compounds containing a mixture of Mn and Cr have the same crystal structure of pure manganites (or chromites), with only Mn (or Cr) in the B site of the perovskite structure. Such an assumption is based on the similar ionic radius of both Cr and Mn ions.[5] The XRD patterns shown in Fig. 2 reveal that the samples are single phase, and all the diffraction peaks were indexed as belonging to the LSCM-*x*% phase. It is important to consider that, similarly to the LSM compounds, LSCM-*x*% exhibits a structural transition depending on the Sr content.[11] The cell parameters and crystalline structure of the LSCM-*x*% samples are listed in Table I. The compounds with $x = 0.3$ and 0.4 have hexagonal crystalline structure, whereas the $x = 0.5$ compound exhibits tetragonal symmetry.[5,9] The calculated lattice parameters of the tetragonal compound (LSCM-50) are $a = b = 5.4354(6)$ Å and $c = 7.682(2)$ Å. Compositions with $x < 0.5$ have calculated lattice parameters $a = b = 5.471(1)$ Å, $c = 13.312(2)$ Å and $a = b = 5.483(2)$ Å, $c = 13.312(3)$ Å for LSCM-40 and LSCM-30, respectively. These values are in good

Table I. Crystalline structure parameters and activation energy values of the LSCM-*x*% compounds.

Sr content (x)	Cell parameters (Å)	Crystal structure	Activation energy (meV)		
			Air		
			$T < 300$°C	$T > 300$°C	Ar/4%H_2
0.3	$a = b = 5.483(2)$ $c = 13.312(3)$	Hexagonal	177	240	556
0.4	$a = b = 5.471(1)$ $c = 13.312(2)$	Hexagonal	175	217	–
0.5	$a = b = 5.4354(6)$ $c = 7.682(2)$	Tetragonal	160	160	–

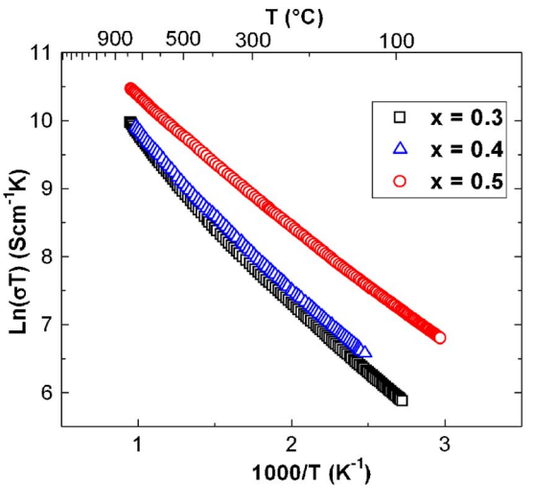

Figure 3. (Color online) Temperature dependence of the electrical conductivity of the LSCM-*x*% (x = 0.3, 0.4, and 0.5) compounds measured in air.

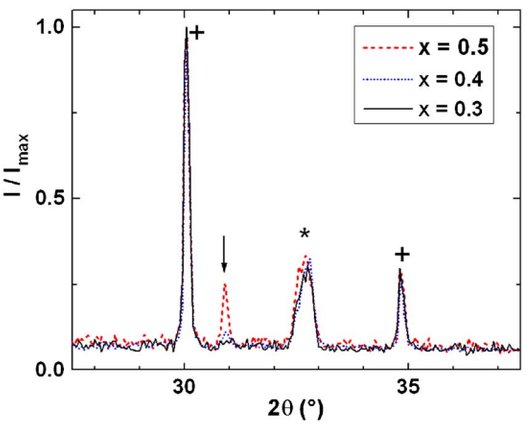

Figure 4. (Color online) XRD patterns of ZrO_2:8 mol % Y_2O_3 and LSCM-*x*% (x = 0.3, 0.4, and 0.5) mixtures treated at 1300°C for 5 h. The ∗ and + symbols mark the main diffraction peaks of the perovskite and electrolyte, respectively. The arrow points to the peak related to the $SrZrO_3$.

agreement with those for LSM and LSCM-*x*% compounds with the same Sr content.[5,11] In addition, it is observed that increasing Sr concentration increases more markedly the lattice parameter a of the crystalline structure, while the c parameter is not significantly changed. Such a feature has been associated with the much smaller size of Mn^{4+} compared to Mn^{3+} and the contracted Mn–O bond length, which compensates the slightly larger Sr^{2+} substituted for La^{3+}.[11]

The temperature dependence of the electrical conductivity [$\sigma(T)$] of the LSCM-*x*% perovskites is shown in Fig. 3. The $\sigma(T)$ and activation-energy values are in good agreement with previously reported data on similar compounds.[4,5] The electrical transport properties of LSCM-*x*% compounds were interpreted in terms of trapping and percolation mechanisms of small polarons.[12,13] The LSCM-*x*% compounds exhibit a thermally activated small polaron-hopping transport, as evidenced by the linear behavior of $\ln(\sigma T)$ in a wide temperature range. The $\sigma(T)$ data displayed in Fig. 3 show that compounds with x = 0.3 and 0.4 exhibit a more clear deviation from the linear behavior for $T > 300$°C than specimens with higher Sr content. Such a smooth activation energy change was associated with a possible phase transition[4] and suggests that no first-order transition occurs.[5] The activation energy (Ea) of the samples was evaluated in both temperature ranges, and the calculated values are shown in Table I. The Ea values were found to be in excellent agreement with previous reported values:[4,5] for $T < 300$°C, Ea = 177 and 175 meV, and for $T > 300$°C, Ea = 240 and 217 meV for the LSCM-30 and LSCM-40 samples, respectively. Increasing the Sr content decreases the activation energy, a feature more pronounced in the $T > 300$°C range. Therefore, further Sr substitution leads to a more linear behavior of $\sigma(T)$ in the whole temperature range investigated, and the sample LSCM-50 exhibits $Ea \approx 160$ meV.

The $\sigma(T)$ data revealed that increasing the Sr content increases the electrical conductivity due to the charge-carrier formation upon oxidation of Mn^{3+} to Mn^{4+}.[8] However, increasing the Sr content also increases the chemical reactivity with zirconia-based electrolytes, as evidenced on the XRD patterns shown in Fig. 4. Similarly to the LSM cathodes, Sr substitutions higher than $x \approx 0.3$ may result in formation of the resistive phase $SrZrO_3$ by the chemical reaction with the electrolyte at high temperatures ($T > 1200$°C).[1]

Based on the above results, the electrical conductivity of the sample LSCM-30 was further investigated in conditions that simulate the operation of an SOFC anode. Two samples from the same batch were submitted up to five redox cycles by performing consecutive $\sigma(T)$ experiments during both heating and cooling in the 100–800°C range, alternating atmosphere between static air and 96% Ar/4% H_2 flow, as displayed in Fig. 5. However, one of the samples was previously heat-treated at 1000°C for 5 h in pure H_2 before the cycling experiments in order to investigate possible aging effects under reducing atmosphere at high temperatures (Fig. 5b). For the sake of clarity, only the first and the last cycles are shown in Fig. 5 for both samples. One important feature is the pronounced decrease of the $\sigma(T)$ and the increase of the activation energy under reducing atmosphere.[4,8] For the sintered sample (Fig. 5a), $\sigma(750°C) \approx 17$ and 0.39 Scm^{-1} in air and gas mixture, respectively. In addition, under reducing atmosphere the activation energy notably increases to Ea = 556 meV, in good agreement with previous data.[8] Increasing the temperature with the reducing gas mixture flowing resembles the $\sigma(T)$ data measured in air (Fig. 3) up to $T \approx 450$°C. However, a rapid decrease of $\sigma(T)$ develops between 450°C up to ~700°C. Further heating above $T \approx 700$°C stabilizes the reduction process, and the thermally activated transport increases $\sigma(T)$ up to the maximum measuring temperature (800°C). Upon cooling, no thermal irreversibility is observed in the 700–800°C temperature range, and the $\sigma(T)$ displays a thermally activated transport with decreasing temperature. However, at $T \approx 150$°C a clear deviation from linear behavior is observed, suggesting a possible phase transition. Such a feature is present for each measurement during cooling in reducing atmosphere for both studied samples, and upon further cooling ($T < 130$°C) the activation energy assumes values similar to those found in experiments in air. Previous XRD analyses at room temperature for the x = 0.25/0.3 compounds indicated that thermal treatment under H_2 results in a hexagonal to orthorhombic/cubic structural transition with small volumetric changes,[5,8] which may be associated with the kink observed in the $\sigma(T)$ curves at $T \approx 150$°C.

Switching the measuring atmosphere from Ar/4% H_2 to air results in a more rapid change of $\sigma(T)$ upon heating, evidencing the more rapid kinetics of the oxidation reaction.[3,5] In fact, for $T > 150$°C, a rapid increase of $\sigma(T)$ coincides with the temperature region of the discussed deviation from linear behavior of $\sigma(T)$ upon cooling in reducing atmosphere. At ~450°C, the oxidation process is complete and the activated transport process in air is resumed, as shown in Fig. 3 and 5.

The data displayed in Fig. 5a and b revealed that the general trends of $\sigma(T)$ during the redox cycles are similar for both samples. However, the sample thermally aged in pure hydrogen exhibits lower values of both $\sigma(T)$ and Ea in both atmospheres (Fig. 5b). In

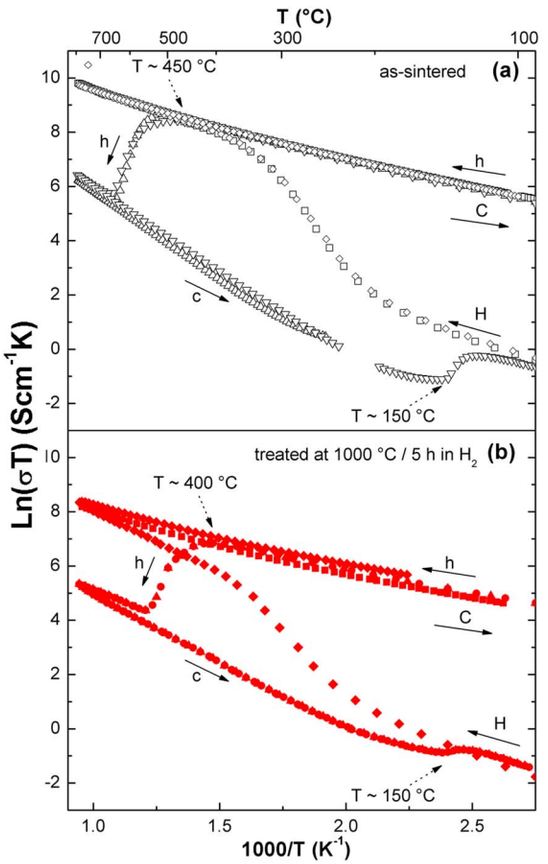

Figure 5. (Color online) Temperature dependence of the electrical conductivity of the $La_{0.7}Sr_{0.3}Cr_{0.5}Mn_{0.5}O_3$ compound measured in air and 96% Ar/4% H_2 gas mixture for both the sintered sample (a) and the sample heat-treated at 1000°C for 5 h under H_2 (b). Solid arrows marked with "h,H" and "c,C" indicate heating and cooling directions, respectively, on both 96% Ar/4% H_2 gas mixture (lowercase letters) and air (capital letters).

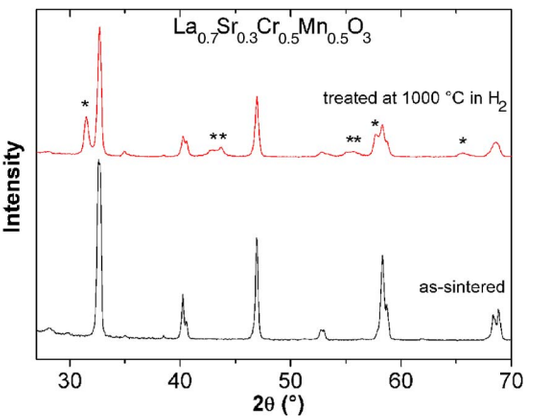

Figure 6. (Color online) Powder XRD patterns of $La_{0.7}Sr_{0.3}Cr_{0.5}Mn_{0.5}O_3$ samples as-sintered and thermally aged under pure hydrogen at 1000°C for 5 h. The ∗ symbol indicates the indexed peaks of the $La_{0.75}Sr_{1.25}MnO_4$ phase (ICSD no. 153649).

fact, the observed aging effects in LSCM-30 seem to be less significant under reducing atmosphere than in air. At 750°C, this specimen shows $\sigma = 2.4$ and 0.18 Scm^{-1} in air and reducing atmosphere, respectively. The *Ea* values for the aged sample are 198 meV (for $T > 300$°C) in air and 427 meV in the gas mixture. For the hydrogen-treated sample (Fig. 5b), the reduction process, visualized as a noticeable decrease of $\sigma(T)$ upon heating in the low $p(O_2)$ atmosphere, occurs at lower T, in the range ~400 to 550°C. A slight thermal irreversibility takes place upon cooling in the 800–550°C region. Further cooling leads to a thermally activated behavior of $\sigma(T)$, and the linear behavior deviation of $\sigma(T)$ is observed at essentially the same temperature, $T \approx 150$°C. However, such a kink on the $\sigma(T)$ data is less pronounced for the hydrogen-aged specimen. When the reduced sample is heated in air, the oxidation, seen as a continuous increase of $\sigma(T)$, occurs along a wider temperature range, and the original $\sigma(T)$ curve is resumed upon cooling in air.

Both samples retain visual integrity after the $\sigma(T)$ measurements, and no appreciable degradation effects are observed on the transport properties for both samples upon redox cycling, revealing the good stability of the ceramic anode in the investigated experimental conditions.

The $\sigma(T)$ data for the sample thermally aged under H_2 was correlated with XRD analysis. Figure 6 shows XRD data for both the as-sintered and the H_2-aged samples. The single-phase LSCM-30 that underwent thermal aging under H_2 at 1000°C for 5 h displays extra peaks, which were found to correspond to the $(La,Sr)_2MnO_4$ oxide, and both phases were found to coexist in the aged sample. The $(La,Sr)_2MnO_4$ oxide has been observed as a possible decomposition product of Sr-substituted $LaMnO_3$ perovskites.[14,15] The $\sigma(T)$ behavior of the aged sample is in good agreement with previous studies that have compared the transport properties of both $(La,Sr)MnO_3$ and $(La,Sr)_2MnO_4$ phases.[15] In that study,[15] it was observed that the p-type electrical conductivity of the $(La,Sr)_2MnO_4$ phase exhibits a much less pronounced decrease at low $p(O_2)$ than in air when compared to the $(La,Sr)MnO_3$ compound, in accordance with the data shown in Fig. 5.

An aging heat-treatment in pure H_2 at 800°C for 5 h resulted in no detectable phase degradation of the LSCM-30 phase, as inferred from XRD analysis (not shown). Such an experimental result is in agreement with the data displayed in Fig. 5, which show no appreciable changes of the electrical conductivity due to redox cycles up to 800°C.

The electrical transport properties are closely related to the defect chemistry of the LSCM-*x*% compounds. Both the reduction and oxidation during heating of the LSCM-*x*% samples observed in the $\sigma(T)$ data can be associated with the oxygen stoichiometry, as inferred from TG data taken in similar conditions.[5] Figure 7 shows the mass variation of the LSCM-30 compound upon heating in both oxidizing and reducing atmosphere. Upon heating under a reducing atmosphere (Ar/4% H_2), the compound sintered in air exhibits a small mass increase due to the buoyancy effect of the experimental apparatus at low temperatures, and no significant mass variation is observed up to ~450°C. Further heating leads to a significant mass loss that starts to develop at $T \sim 450$°C, and a rapid reduction is observed in the 500–750°C range. Above $T \approx 750$°C the mass-loss rate is reduced, indicating that the reduction process tends to stabilize at higher temperatures. In the investigated temperature range, the total mass loss is ~0.5 mg, which corresponds to ~1% of the initial value. After cooling down to room temperature under reducing conditions, the atmosphere was switched to air and the mass gain was recorded during heating. With increasing temperature in air, the sample exhibits a relatively slow mass gain due to oxygen uptake. The oxidation process starts to develop at relatively lower temperatures ($T \geq 250$°C) and stabilizes at temperatures close to the ones in which the reduction process starts ($T \approx 500$°C). TG analysis closely resembles the behavior of $\sigma(T)$ data under both reducing and oxidizing processes, and both experiments indicate the faster kinetics of the oxidation reaction. In addition, the TG data

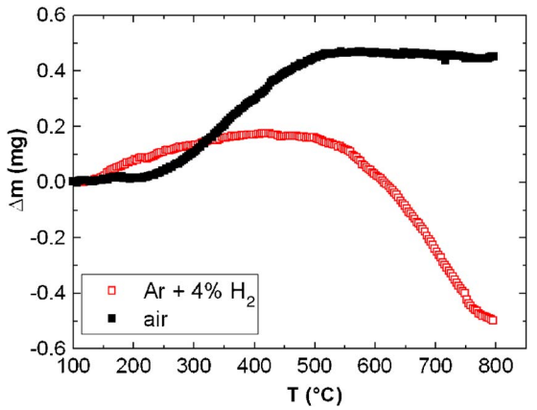

Figure 7. (Color online) TG analysis of the $La_{0.7}Sr_{0.3}Cr_{0.5}Mn_{0.5}O_3$ compound measured during heating under air (solid symbols) and 96% Ar/4% H_2 gas mixture (open symbols).

present similar mass variation upon oxidation and reduction that corresponds to ~1 wt % of the total mass, providing further evidence of the redox stability of the compound.

These analyses are in good agreement with previous TG data recorded during the oxidation of reduced samples of LSCM-25, which revealed a similar mass uptake (1 wt %) that corresponds to 0.25 per formula unit of oxygen.[5] Recently, X-ray absorption techniques indicated that charge carriers are associated with Mn^{4+} and that Cr retains the 3+ oxidation state upon Sr doping in LSCM-*x*% compounds.[8] In air, Sr doping increases the small polaron concentration, resulting in high electrical conductivity. At low $p(O_2)$, charge compensation is achieved by the formation of oxygen vacancies, decreasing the p-type charge carrier concentration and reducing the electronic conductivity.[5]

Conclusions

The perovskite phase LSCM-*x*% was successfully synthesized by the citrate technique. Single-phase compounds were obtained after sintering at 1400°C. Both the electrical conductivity and the chemical reactivity with zirconia-based electrolytes increased with increasing Sr content. Similarly to strontium-doped lanthanum manganite cathodes, a safe limit for the Sr substitution is ~30 atom % in order to avoid significant reaction with the electrolyte. The redox stability of the ceramic anode was evaluated up to five cycles between temperatures ranging from 100°C to those of SOFC operation (800°C). However, thermal aging at 1000°C under pure hydrogen has shown some degradation effects on the transport properties of the perovskite that were less pronounced in reducing atmosphere and related to the decomposition of the perovskite phase. The presented results suggest that further microstructural optimization may be needed in order to improve the perovskite properties for application as the SOFC anode.

Acknowledgments

This research was supported by the Brazilian agencies FAPESP (04/09803-3) and CNPq (301661/2004-9 and 504562/2004-5). Thanks are also due to CNEN for a Probic scholarship (103343/2005-9) and to Dr. E. V. Spinace (IPEN) for helping us with heat-treatments in H_2.

Instituto de Pesquisas Energéticas e Nucleares assisted in meeting the publication costs of this article.

References

1. S. C. Singhal and K. Kendall, *High Temperature Solid Oxide Fuel Cells–Fundamentals, Design and Applications*, p. 1, Elsevier, New York (2004).
2. A. Atkinson, S. Barnett, R. J. Gorte, J. T. S. Irvine, A. J. Mcevoy, M. Mogensen, S. C. Singhal, and J. Vohs, *Nat. Mater.*, **3**, 17 (2004).
3. J. W. Fergus, *Solid State Ionics*, **177**, 1529 (2006).
4. S. Tao and J. T. S. Irvine, *Nat. Mater.*, **2**, 320 (2003).
5. S. Tao and J. T. S. Irvine, *J. Electrochem. Soc.*, **151**, A252 (2004).
6. S. Zha, P. Tsang, Z. Cheng, and M. Liu, *J. Solid State Chem.*, **178**, 1844 (2005).
7. S. P. Jiang, X. J. Chen, S. H. Chan, J. T. Kwok, and K. A. Khor, *Solid State Ionics*, **177**, 149 (2006).
8. S. M. Plint, P. A. Connor, S. Tao, and J. T. S. Irvine, *Solid State Ionics*, **177**, 2005 (2006).
9. R. Muccillo, E. N. S. Muccillo, I. C. Cosentino, F. C. Fonseca, Y. Vidoto, and N. H. Saito, *Mater. Sci. Forum*, **299-300**, 80 (1999).
10. C. N. Chervin, B. J. Clapsaddle, H. W. Chiu, A. E. Gash, J. H. Satcher Jr., and S. M. Kauzlarich, *Chem. Mater.*, **18**, 1928 (2006).
11. A. Hammouche, E. Siebert, and A. Hammou, *Mater. Res. Bull.*, **24**, 367 (1989).
12. R. Raffaelle, H. U. Anderson, D. M. Sparlin, and P. E. Parris, *Phys. Rev. B*, **43**, 7991 (1991).
13. R. Raffaelle, H. U. Anderson, D. M. Sparlin, and P. E. Parris, *Phys. Rev. Lett.*, **65**, 1383 (1990).
14. Q. X. Fu, F. Tietz, P. Lersch, and D. Stöver, *Solid State Ionics*, **177**, 1059 (2006).
15. M. Al Daroukh, V. V. Vashook, H. Ullmann, F. Tietz, and I. Arual Raj, *Solid State Ionics*, **158**, 141 (2003).